Received May 29, 2018, accepted July 9, 2018, date of publication July 13, 2018, date of current version August 7, 2018.

Digital Object Identifier 10.1109/ACCESS.2018.2855697

Multi-Objective Coordinated Planning of Active-Reactive Power Resources for Decentralized Droop-Controlled Islanded Microgrids Based on Probabilistic Load Flow

ZEHUAI LIU[1], JIAHAO YANG[2], YONGJUN ZHANG[1], TIANYAO JI[1], JUNHUANG ZHOU[1], AND ZEXIANG CAI[1]

[1]School of Electric Power, South China University of Technology, Guangzhou 510630, China
[2]School of Mechanical and Electrical Engineering, Xiamen University Tan Kah Kee College, Zhangzhou 363105, China

Corresponding author: Yongjun Zhang (zhangjun@scut.edu.cn)

This work was supported in part by the National Natural Science Foundation of China under Grant 51777077 and in part by the Natural Science Foundation of Guangdong Province under Grant 2017A030313304.

ABSTRACT The intermittency of distributed generation and the fluctuation of load will derive uncertainties to the decentralized droop-controlled islanded microgrids (IMGs) operation. In order to describe and analyse the probabilistic characteristics of the operating state of an IMG, this paper proposes an analytical method based on cumulants to solve the probabilistic load flow (PLF) for decentralized droop-controlled IMGs, considering the correlation of input variables. Nataf transform is used to deal with the correlation, and the PLF is solved using the cumulant method and the Gram-Charlier series expansion. On this basis, a multi-objective coordinated planning model of active-reactive power resources is presented, considering the annual comprehensive cost and operating risk simultaneously. The Pareto optimal solution set is found using non-dominated sorting genetic algorithm-II to provide a set of alternative planning schemes. The proposed PLF based on cumulant method is compared with Monte Carlo simulation to verify its accuracy and efficiency. Besides, the simulation results also demonstrate that the proposed coordinated planning model of active-reactive power resources can coordinate the security and economy of the IMG operation.

INDEX TERMS Multi-objective planning, decentralized droop-controlled islanded microgrid, cumulant, probabilistic load flow.

NOMENCLATURE

CONSTANTS

d	Discount rate
n	Number of buses
$T_{\text{sys}}^{\text{use}}$	System annual operating hours
T_{con}	Continuous operating hours in the maximum Charge/discharge power of ESS

SETS

Ω_{B}	Set of bus indices
Ω_{L}	Set of branch indices

VARIABLES

$P_{\text{C}i}$, $Q_{\text{C}i}$	Active and reactive power generated by the DGs that generate constant power at bus i
$P_{\text{D}i}$, $Q_{\text{D}i}$	Active and reactive power generated by droop-controlled units at bus i
$P_{\text{L}i}$, $Q_{\text{L}i}$	Active and reactive power of load at bus i
Δf, $\Delta\,\delta$, $\Delta \boldsymbol{U}$	Corrections of frequency, bus voltage angles and magnitudes
$\boldsymbol{J}$	Jacobian matrix
$K_{\text{D}fi}$, $K_{\text{D}Ui}$	Frequency droop gain and bus voltage droop gain

2169-3536 © 2018 IEEE. Translations and content mining are permitted for academic research only.
Personal use is also permitted, but republication/redistribution requires IEEE permission.
See http://www.ieee.org/publications_standards/publications/rights/index.html for more information.

U_i, U_j Voltage magnitude of bus i and bus j

G_{ij}, B_{ij} Real part and imaginary part of node admittance matrix

δ_{ij} Voltage phase angle difference of bus i and bus j

$P^{r}_{MTG\_i}$, $P^{r}_{WTG\_i}$, $P^{r}_{PVG\_i}$, $E^{r}_{ESS\_i}$, $Q^{r}_{DS\_i}$ Installation capacity of MTG, WTG, PVG, ESS, DSTATCOM at bus i

P_{MTG_i}, P_{WTG_i}, P_{PVG_i}, P_{ESS_i}, Q_{DS_i} Active power of MTG, WTG, PVG, ESS and the reactive power of DSTATCOM at bus i

Q_{MTG_i}, Q_{WTG_i}, Q_{PVG_i} Reactive power of MTG, WTG, PVG at bus i

PARAMETERS

$c^{I}_{MTG\_i}$, $c^{I}_{WTG\_i}$, $c^{I}_{PVG\_i}$, $c^{I}_{ESS\_i}$, $c^{I}_{DS\_i}$ Fixed investment cost per unit capacity of MTG, WTG, PVG, ESS, DSTATCOM at bus i

y_{MTG}, y_{WTG}, y_{PVG}, y_{ESS}, y_{DS} Economic life of MTG, WTG, PVG, ESS, and DSTATCOM

$c^{OM}_{MTG\_i}$, $c^{OM}_{WTG\_i}$, $c^{OM}_{PVG\_i}$ Operation and maintenance cost per unit generated energy of MTG, WTG and PVG at bus i

$c^{OM}_{ESS\_i}$, $c^{OM}_{DS\_i}$ Operation and maintenance cost per unit capacity of ESS and DSTATCOM at bus i

$c^{F}_{MTG\_i}$ Fuel cost per unit generated energy of MTG

c_{Loss} Price of loss

R_{Ui} Probability of over-limit voltage at bus i,

R_{Sl} Probability of over-limit power transmitted on branch l

R_F Probability of over-limit frequency

f_{max}, f_{min} The maximum and minimum allowable frequency

U_{imax}, U_{imin} The maximum and minimum allowable voltage at bus i

γ_U, γ_S, γ_F The confidence of voltage, branch power and frequency

ABBREVIATIONS

DG	Distributed generation
MGs	Microgrids
IMGs	Islanded microgrids
NSGA-II	Non-dominated sorting genetic algorithm-II
LF	Load flow
PLF	Probabilistic load flow
PLFCM	Probabilistic load flow based on cumulant method
MCS	Monte Carlo simulation
ESSs	Energy storage systems
PVG	Photovoltaic generation
WTG	Wind turbine generation
MTG	Micro gas turbine generation
PDF	Probability distribution function
CDF	Cumulative distribution function
NR	Newton Raphson

I. INTRODUCTION

Due to the extensive DG integration, the operation and planning of distribution system become more and more challenging [1]. The microgrids (MGs), which are composed of DG, distributed energy storage systems (ESSs) and flexible load, provide an important technical means for the comprehensive utilization of DG [2]–[4]. According to whether they are connected to the main network, MGs can be classified into grid-connected MGs and IMGs. As IMGs do not have slack bus and are lack of support from the main network, their operating characteristic is different from that of distribution systems or grid-connected MGs. Two operating schemes have been proposed for IMGs operation, which are centralized control schemes and decentralized droop control schemes [5], [6]. Centralized control schemes require a MG central controller to manage and control the IMG [7], and has a strong dependence on the performance of the MG central controller and communication infrastructure, which are found to be both costly and unreliable [5]. Unlike centralized control schemes, decentralized droop control schemes require only local measurements to achieve appropriate sharing of the load demand among the different active-reactive power resources in the IMG and to control the voltage and frequency [5], [8], [9]. This in turn makes IMG operation independent of centralized communication and the droop-controlled units are easy to plug and play [5]. In view of the advantage of decentralized droop control schemes mentioned above, this paper mainly focuses on decentralized droop-controlled IMGs (here, decentralized droop-controlled

IMGs refers to the IMGs that use the decentralized droop control as the operating scheme [5]).

Load flow (LF) calculation is the foundation of the planning and operation of IMGs [10]. However, the intermittency of photovoltaic generation (PVG) and wind turbine generation (WTG), as well as the fluctuation of load, make it difficult to fully evaluate the operating state of the IMG by single scenario LF. To solve this, PLF evaluation is an important approach to investigate the characteristics under an uncertain environment on account of the probability distribution information of each output variable that can be obtained.

Three types of methods are generally used for PLF calculation, which are MCS [11], [12], point estimate method [13], [14] and cumulant method [15], [16]. MCS relies on a large sampling scale; nonetheless there are some methods that can improve the efficiency of sampling such as Latin hypercube sampling [11]. MCS is applied in [12] for PLF calculation in a decentralized droop-controlled IMG. Considering LF calculation of IMG is complex and with a slow convergence speed, PLF calculation for IMG based on MCS is unpractical for online application, as MCS may result in huge computational burden [17]. The disadvantages of point estimate method are that: first, point estimate method cannot provide the probability distribution function (PDF) of the output variables [18]; second, it becomes less accurate as the correlation of input variables increases [19]. In [20] and [21], the uncertainties of DG and load are taken into account, and point estimation method [20] and cumulant method [21] are introduced to calculate the PLF for evaluating the operating state of a grid-connected MG. However, in a grid-connected MG, the point of common coupling where the MG is connected to the main network is treated as a slack bus; thus, its PLF model is similar to that of a distribution system. For decentralized droop-controlled IMGs, their PLF model is much different from that of distribution systems or grid-connected MGs. Thus, the conventional methods for PLF are not suitable for them. Cumulant method has high computational efficiency because it only needs to perform the LF calculation once at the operating point [22]. It seems that PLFCM is particularly suitable to be embedded in intelligent optimization algorithms to solve the chance constraint optimization model due to its low computational burden. Moreover, its accuracy could meet the requirement of engineering application. However, for decentralized droop-controlled IMGs, no research work has been reported on using cumulant method for PLF.

The active-reactive power resource planning of an IMG is different from that of a grid-connected MG or an active distribution network. An IMG has higher requirements in matching generation and load and regulating active and reactive power. Moreover, the operating schemes of the IMG directly influence the power outputs of active-reactive power resources, which inevitably affects their planning result. For the decentralized droop-controlled IMG, the active power resources mainly include DG and ESSs. Considering the operating requirement of reactive power dynamic adjustment and the need of droop control, DSTATCOM [23], [24] is generally selected as the reactive power resource. Active-reactive power resource planning generally includes choosing the installation position, determining the installation capacity, or location and sizing.

There is little literature on IMG planning, and most of the research focuses on the planning of active power resources. In [25], a tri-level expansion planning framework is presented for an IMG and the uncertainties of load forecasting are considered. Meanwhile, Latin hypercube sampling is used to generate the load demand scenarios. In [26], a model for MG planning with uncertain physical and financial information is presented, in which robust optimization approach is adopted to consider the errors of load forecast and varying renewable generation. The uncertainties of DG power output and the fluctuation of load in [27] are classified into 4 seasonal scenarios, and a DG sizing method in MG considering economy and reliability is proposed. In [28], an optimal planning model for IMG is presented based on its possible operating scenarios and the reliability evaluation models, with the objective of minimizing the present values of the costs, and with the constraints of system operation and reliability. In [29], PV power is classified into several scenarios according to different weather conditions, and a methodology for the optimal allocation and economic analysis of ESS in MG based on net present value is presented.

The research works presented above are based on scenarios generated by sampling, which to some extent can reflect the uncertainties of DG and load. However, for an IMG, there are many units such as PVG, WTG, ESS, micro gas turbine generation (MTG) and DSTATCOM, thus its planning is a multi-variable, strong correlation process. As a result, using scenarios generated by sampling for IMG planning may face the following challenges. On one hand, it is difficult to use several typical scenarios to fully reflect the operating state of the MG. On the other hand, it causes unbearable computational burden if many scenarios are used. In addition, from the viewpoint of risk control, the methods for IMG planning mentioned above are mainly concerned with power balance, whereas the operating risk caused by over-limit of voltage and frequency is not considered. Moreover, the operating characteristics of decentralized droop control are not considered for IMG planning either.

The major contributions of this paper are summarized as follows. In order to fully evaluate and analyse the operating state of a decentralized droop-controlled IMG in an uncertainty environment, PLFCM is proposed, and the correlation among DG power outputs is considered. Furthermore, a multi-objective coordinated planning model of active-reactive power resources in a decentralized droop-controlled IMG is proposed to control the annual comprehensive cost and the operating risk. Meanwhile, the proposed PLFCM is embedded in NSGA-II to solve the multi-objective planning model.

The rest of the paper is organized as follows: PLFCM for decentralized droop-controlled IMGs is proposed

in Section II. Multi-objective coordinated planning model of active-reactive power resources based on two aspects of benefits and risks conditions is presented in Section III. Simulation studies are given in Section IV. Conclusions are outlined in Section V.

II. PLF FOR DECENTRALIZED DROOP-CONTROLLED IMGS

A. MODELLING OF LF FOR DECENTRALIZED DROOP-CONTROLLED IMGs

The bus types in IMG LF calculation can be classified into PQ bus, PV bus and droop bus [5], 1[0]. The conventional droop control method is based on the power flow theory in an alternating current system. The theory states that if impedances between sources are highly inductive, the active power is predominantly controlled by the frequency, whereas the reactive power is predominantly controlled by the voltage magnitude [30]. Since most of the active-reactive power resources in an IMG have a power inverter interface followed by a filter with the large inductor, it is justified to assume the output impedance of the active-reactive power resources to be inductive [10], [30]. The power equation of an arbitrary bus can be uniformly expressed as

$$\begin{cases} \Delta P_i = P_{\mathrm{C}i} + P_{\mathrm{D}i} - P_{\mathrm{L}i} - P_i \\ \Delta Q_i = Q_{\mathrm{C}i} + Q_{\mathrm{D}i} - Q_{\mathrm{L}i} - Q_i \end{cases} \tag{1}$$

where $P_{\mathrm{C}i}$ and $Q_{\mathrm{C}i}$ respectively represent the active and reactive power generated by the DGs that generate constant power at bus i, such as PVG and WTG that adopt MPPT control mode; $P_{\mathrm{D}i}$ and $Q_{\mathrm{D}i}$ respectively represent the active and reactive power generated by droop-controlled units at bus i, such as MTG, ESS and DSTATCOM; $P_{\mathrm{L}i}$ and $Q_{\mathrm{L}i}$ respectively represent the active and reactive power of load at bus i; P_i and Q_i respectively represent the injected active and reactive power at bus i; ΔP_i and ΔQ_i are the mismatches of injected active and reactive power at bus i, respectively.

In addition, other control methods, such as virtual inertia based control and virtual synchronous machine based control, can also be implemented for decentralized droop-controlled IMGs. In terms of steady-state operation, when the units that adopt virtual inertia based control or virtual synchronous machine based control participate in frequency regulation, their operating characteristic is similar to that of the units adopting droop control [31], [32]. Hence the bus where the units adopting virtual inertia based control or virtual synchronous machine based control are connected can also be treated as droop bus for LF calculation.

The expression of $P_{\mathrm{D}i}$, $Q_{\mathrm{D}i}$, $P_{\mathrm{L}i}$, $Q_{\mathrm{L}i}$, P_i, Q_i can be found in formulae (1), (2), (7), (8), (11), (12) of [33] respectively.

For the nonlinear equations shown in (1), the mismatch equations can be formulated as

$$\begin{bmatrix} \Delta \boldsymbol{P} \\ \Delta \boldsymbol{Q} \end{bmatrix} = \boldsymbol{J} \cdot \begin{bmatrix} \Delta f \\ \Delta \boldsymbol{\delta} \\ \Delta \boldsymbol{U} \end{bmatrix} = \begin{bmatrix} \boldsymbol{E} & \boldsymbol{H} & \boldsymbol{N} \\ \boldsymbol{F} & \boldsymbol{M} & \boldsymbol{L} \end{bmatrix} \cdot \begin{bmatrix} \Delta f \\ \Delta \boldsymbol{\delta} \\ \Delta \boldsymbol{U} \end{bmatrix} \tag{2}$$

where $\Delta \boldsymbol{P}$ and $\Delta \boldsymbol{Q}$ are the mismatch vectors of injected active and reactive power respectively; Δf, $\Delta \boldsymbol{\delta}$ and $\Delta \boldsymbol{U}$ are the corrections of frequency, bus voltage angles and magnitudes; $\boldsymbol{J}$ is the Jacobian matrix, in which partition matrices are defined as

$$\begin{aligned} \boldsymbol{E} &= \frac{\partial \Delta \boldsymbol{P}}{\partial f} \boldsymbol{H} = \frac{\partial \Delta \boldsymbol{P}}{\partial \boldsymbol{\delta}} \boldsymbol{N} = \frac{\partial \Delta \boldsymbol{P}}{\partial \boldsymbol{U}} \\ \boldsymbol{F} &= \frac{\partial \Delta \boldsymbol{Q}}{\partial f} \boldsymbol{M} = \frac{\partial \Delta \boldsymbol{Q}}{\partial \boldsymbol{\delta}} \boldsymbol{L} = \frac{\partial \Delta \boldsymbol{Q}}{\partial \boldsymbol{U}} \end{aligned} \tag{3}$$

The expressions of partition matrices are detailed in Appendix A.

Traditionally the nonlinear equations of the LF problem are solved using the Newton Raphson (NR) method. However, it faces several challenges when applied to IMGs, because there is no slack bus [5]. For example, the NR method may fail to get a solution even if it starts from a flat initial guess, because the region of the LF solution of IMGs is too narrow [5]. Besides, the NR method usually fails to solve the nonlinear equations of LF due to the singularity of the Jacobian matrix, which is caused by the fact that the region of the LF solution of IMGs is so narrow that the operating point of stability is close to the boundary of collapse. To tackle these demerits, in this paper, the Newton trust-region method, which is proposed in [5] and [6], is used to solve the nonlinear equations. The specific implementation process is shown in [6], and the flowchart can be found in [6, Fig. 6].

B. PLFCM FOR DECENTRALIZED DROOP-CONTROLLED IMGs

1) MODELING OF UNCERTAINTIES

The most widely adopted method to describe the uncertainties of WTG and PVG power output are to assume that wind speed follows the Weibull distribution, and solar radiation follows the Beta distribution [11]–[14]. The PDF of the wind speed and the wind power output can be formulated as formulae (4)-(5) in [34], respectively. The PDF of solar radiation and the output of a PVG unit can be described by formulae (6)-(7) in [34]. Generally, normal distribution is used to describe the fluctuation of load. The PDF of load is expressed as formula (10) in [34].

Since IMGs are independent small systems and each PVG unit or WTG unit is installed closely to one another, their power output has a strong correlation. In addition, there is a correlation between wind speed and solar radiation in the same area. Considering the complementarity of WTG-PVG, the correlation coefficient is negative [35]. The correlation coefficient matrix can be denoted as

$$\rho = \begin{bmatrix} 1 & \rho_{\mathrm{wp}} \\ \rho_{\mathrm{pw}} & 1 \end{bmatrix} \tag{4}$$

where ρ_{wp} and ρ_{pw} are the correlation coefficients between WTG and PVG.

Given m input random variables $\boldsymbol{W}=[w_1, w_2, \ldots, w_m]$, the correlation coefficient matrix $\boldsymbol{R}_{\boldsymbol{W}}$ is used to describe

the correlation:

$$R_W = \begin{bmatrix} 1 & \rho_{w_{12}} & \cdots & \rho_{w_{1m}} \\ \rho_{w_{21}} & 1 & \cdots & \rho_{w_{2w}} \\ \vdots & \vdots & \vdots & \cdots \\ \rho_{w_{m1}} & \rho_{w_{m2}} & \cdots & 1 \end{bmatrix} \tag{5}$$

where $\rho_{w_{ij}}$ are the correlation coefficients between $w_i$and w_j.

C. CUMULANT METHOD

In this paper, the cumulant method is applied to solve the PLF. The steps are given as follows.

Step 1: Based on the modeling of the uncertainties of PVG, WTG and load, as mentioned above, the random characteristics of DG output power and load are obtained, that is, m random variables, denoted by $\boldsymbol{W}$, are obtained.

Step 2: According to formula (5), the correlation coefficient matrix $\boldsymbol{R_W}$ is obtained.

Step 3: According to the cumulative distribution function (CDF) of the input random variables and correlation coefficient matrix$\boldsymbol{R_W}$, the correlation coefficient matrix $\boldsymbol{R_Y}$ of the sample matrix $\boldsymbol{Y}$, which follows the standard normal distribution can be obtained.

Step 4: Apply Cholesky decomposition to $\boldsymbol{R_Y}$ to obtain the lower triangular matrix $\boldsymbol{D_Y}$.

Step 5: Obtain the independent sample matrix $\boldsymbol{S}$ by sampling the m independent standard normal random variables, and then calculate $\boldsymbol{Y}$from $\boldsymbol{Y}$=$\boldsymbol{D_Y S}$.

The specific process of Step1-Step5 can be found in [36].

Step 6: Apply Cholesky decomposition to $\boldsymbol{R_W}$ to obtain the lower triangular matrix $\boldsymbol{D_W}$, and m independent variables $\boldsymbol{W_{ind}}$ can be obtained [22]:

$$W_{\text{ind}} = D_W^{-1} W \tag{6}$$

Step 7: Perform deterministic LF calculation at the operating point to obtain the Jacobian matrix $\boldsymbol{J_0}$.

Step 8: Given each order cumulants of $\boldsymbol{W}$, each order cumulants of $\boldsymbol{W_{ind}}$ can be obtained through formula (6). And $\boldsymbol{J_0}$ should be revised by $\boldsymbol{D_W}$ [22].

Step 9: Linearizing (1) at the operating point and omitting the terms which are higher than the second order, the equation system becomes

$$\begin{cases} \boldsymbol{\Delta X} = \boldsymbol{J}_0^{-1} \boldsymbol{\Delta W} = \boldsymbol{L} \Delta \boldsymbol{W} \\ \boldsymbol{\Delta Z} = \boldsymbol{G}_0 J_0^{-1} \boldsymbol{\Delta W} = \boldsymbol{K} \Delta \boldsymbol{W} \\ \boldsymbol{G}_0 = (\partial \boldsymbol{Z} / \partial \boldsymbol{X})|_{X=X_0} \end{cases} \tag{7}$$

where $\Delta \boldsymbol{W}$ are the uncertainty variable vectors of injected active and reactive power, $\Delta \boldsymbol{X}$ are the uncertainty variable vectors of frequency, bus voltage angles and magnitudes, $\Delta \boldsymbol{Z}$ are the uncertainty variable vectors of branch transmitted power. $\boldsymbol{L}$, $\boldsymbol{K}$are the sensitivity matrices of $\Delta \boldsymbol{X}$and $\Delta \boldsymbol{Z}$, respectively.

Formula (1) includes the power of the droop-controlled units, which is related to the frequency and the bus voltage. In order to obtain the probability distribution of the output power of droop-controlled units, its cumulants should be calculated. Formulae (1) and (2) of [33] represent the frequency and voltage equations of the droop bus. Linearizing formulae (1) and (2) of [33] at the operating point, we have

$$\begin{cases} \Delta P_{\text{D}i} = -\dfrac{1}{K_{\text{D}fi}} \Delta f \\ \Delta Q_{\text{D}i} = -\dfrac{1}{K_{\text{D}Ui}} \Delta U_i \end{cases} \tag{8}$$

where $K_{\text{D}fi}$ and $K_{\text{D}Ui}$ respectively represent frequency droop gain and bus voltage droop gain.

The expression of $K_{\text{D}fi}$ and $K_{\text{D}ui}$ is as follows [5]:

$$\begin{cases} K_{\text{D}fi} = \dfrac{f_{\max} - f_{\min}}{P_{\text{D}i\max} - P_{\text{D}i\min}} \\ K_{\text{D}Ui} = \dfrac{U_{i\max} - U_{i\min}}{Q_{\text{D}i\max} - Q_{\text{D}i\min}} \end{cases} \tag{9}$$

where $f_{\max}$ and $f_{\min}$ are the maximum and minimum allowable frequency; $U_{i\max}$ and $U_{i\min}$ are the maximum and minimum allowable voltage at bus i; $P_{\text{D}i\max}$ and $P_{\text{D}i\min}$ are the maximum and minimum active power capability of the droop-controlled units at bus i; $Q_{\text{D}i\max}$ and $Q_{\text{D}i\min}$ are the maximum and minimum reactive power capability of the droop-controlled units at bus i.

As the uncertainty variable vectors of injected active and reactive power of droop-controlled units is obtained by formula (8), each order cumulants of$\boldsymbol{X}$, $\boldsymbol{Z}$ can be obtained by formula (7).

Step 10: Based on Gram-Charlier series expansion [16], the PDF and CDF of frequency, bus voltage and branch power can be obtained.

In addition, as the grid being resistive or inductive has something to do with active-reactive power-sharing [30], it will influence the expression of $P_{\text{D}i}$ and $Q_{\text{D}i}$ of formula (1) in this paper, and consequently it will influence the power equation of PLF. However, for PLF calculation in the resistive grid, we only need to use formulae (7) and (8) in [10] to express $P_{\text{D}i}$ and $Q_{\text{D}i}$, respectively, and transform ω to f by $f = \frac{\omega}{2\pi}$. Thus the corresponding elements of the Jacobian matrix should be changed as well. That is, whether the grid is resistive or inductive merely influences the corresponding elements of the Jacobian matrix, and has nothing to do with the method of PLF. Hence, the proposed PLFCM is also appropriate for resistive grids.

III. MULTI-OBJECTIVE CHANCE-CONSTRAINED PLANNING OF ACTIVE-REACTIVE POWER RESOURCES FOR DECENTRALIZED DROOP-CONTROLLED IMGS

In this paper, a multi-objective chance constraint planning model of the active-reactive power resources is proposed targeting at two aspects: minimum annual comprehensive cost and minimum operating risk of the IMG. Active resources include DG and ESS, where DG involves MTG, WTG, and PVG, and reactive resource refers to DSTATCOM.

A. OBJECTIVE FUNCTIONS

This paper designs objective functions of annual comprehensive cost and the operating risk of IMGs.

1) ANNUAL COMPREHENSIVE COST

Annual comprehensive cost includes: equivalent annual investment costs of DG, ESS and DSTATCOM, C_{I}; operation and maintenance cost of DG, ESS and DSTATCOM, C_{OM}; fuel cost, C_{F}; annual loss cost, C_{Loss}. The expression of annual comprehensive cost is described as follows:

$$f_1 = C_{\mathrm{I}} + C_{\mathrm{OM}} + C_{\mathrm{F}} + C_{\mathrm{Loss}} \tag{10}$$

The expressions of C_{I}, C_{OM}, C_{F}, C_{Loss}, are shown by formulae (11)-(14):

$$\begin{aligned} C_{\mathrm{I}} = {} & \frac{d(1+d)^{y_{\mathrm{MTG}}}}{(1+d)^{y_{\mathrm{MTG}}}-1}\sum_{i=1}^{n}(c^{\mathrm{I}}_{\mathrm{MTG}\_i}P^{\mathrm{r}}_{\mathrm{MTG}\_i}) \\ & + \frac{d(1+d)^{y_{\mathrm{WTG}}}}{(1+d)^{y_{\mathrm{WTG}}}-1}\sum_{i=1}^{n}(c^{\mathrm{I}}_{\mathrm{WTG}\_i}P^{\mathrm{r}}_{\mathrm{WTG}\_i}) \\ & + \frac{d(1+d)^{y_{\mathrm{PVG}}}}{(1+d)^{y_{\mathrm{PVG}}}-1}\sum_{i=1}^{n}(c^{\mathrm{I}}_{\mathrm{PVG}\_i}P^{\mathrm{r}}_{\mathrm{PVG}\_i}) \\ & + \frac{d(1+d)^{y_{\mathrm{Ess}}}}{(1+d)^{y_{\mathrm{ESS}}}-1}\sum_{i=1}^{n}(c^{\mathrm{I}}_{\mathrm{ESS}\_i}E^{\mathrm{r}}_{\mathrm{ESS}\_i}) \\ & + \frac{d(1+d)^{y_{\mathrm{DS}}}}{(1+d)^{y_{\mathrm{DS}}}-1}\sum_{i=1}^{n}(c^{\mathrm{I}}_{\mathrm{DS}\_i}Q^{\mathrm{r}}_{\mathrm{DS}\_i}) \end{aligned} \tag{11}$$

$$\begin{aligned} C_{\mathrm{OM}} = {} & \sum_{i=1}^{n}(c^{\mathrm{OM}}_{\mathrm{MTG}\_i}E_{\mathrm{MTG}\_i} + c^{\mathrm{OM}}_{\mathrm{WTG}\_i}E_{\mathrm{WTG}\_i} \\ & + c^{\mathrm{OM}}_{\mathrm{PVG}\_i}E_{\mathrm{PVG}\_i} + c^{\mathrm{OM}}_{\mathrm{ESS}\_i}E^{\mathrm{r}}_{\mathrm{ESS}\_i} + c^{\mathrm{OM}}_{\mathrm{DS}\_i}Q^{\mathrm{r}}_{\mathrm{DS}\_i}) \end{aligned} \tag{12}$$

$$C_{\Gamma} = \sum_{i=1}^{n}(c^{\Gamma}_{\mathrm{MTG}\_i}E_{\mathrm{MTG}\_i}) \tag{13}$$

$$C_{\mathrm{Loss}} = c_{\mathrm{Loss}}P^{\mathrm{xp}}_{\mathrm{Loss}}T^{\mathrm{se}}_{\mathrm{sys}} \tag{14}$$

where d is the discount rate; n is the number of buses; $y_{\mathrm{MTG}}, y_{\mathrm{WTG}}, y_{\mathrm{PVG}}, y_{\mathrm{ESS}}, y_{\mathrm{DS}}$ respectively represent economic life of MTG, WTG, PVG, ESS, and DSTATCOM; $c^{\mathrm{I}}_{\mathrm{MTG}\_i}$, $c^{\mathrm{I}}_{\mathrm{WTG}\_i}$, $c^{\mathrm{I}}_{\mathrm{PVG}\_i}$, $c^{\mathrm{I}}_{\mathrm{ESS}\_i}$, $c^{\mathrm{I}}_{\mathrm{DS}\_i}$ are the fixed investment cost per unit capacity of MTG, WTG, PVG, ESS, DSTATCOM at bus i, respectively; $P^{\mathrm{r}}_{\mathrm{MTG}\_i}, P^{\mathrm{r}}_{\mathrm{WTG}\_i}, P^{\mathrm{r}}_{\mathrm{PVG}\_i}, E^{\mathrm{r}}_{\mathrm{ESS}\_i}, Q^{\mathrm{r}}_{\mathrm{DS}\_i}$ are the installation capacity of MTG, WTG, PVG, ESS, DSTATCOM at bus i, respectively; $c^{\mathrm{OM}}_{\mathrm{MTG}\_i}$, $c^{\mathrm{OM}}_{\mathrm{WTG}\_i}$, $c^{\mathrm{OM}}_{\mathrm{PVG}\_i}$ are the operation and maintenance cost per unit generated energy of MTG, WTG and PVG at bus i, respectively; $c^{\mathrm{OM}}_{\mathrm{ESS}\_i}$, $c^{\mathrm{OM}}_{\mathrm{DS}\_i}$ are the operation and maintenance cost per unit capacity of ESS and DSTATCOM at bus i, respectively; $E_{\mathrm{MTG}\_i}, E_{\mathrm{WTG}\_i}$, E_{PVG_i} are annual generated energy of MTG, WTG, PVG at bus i, respectively; $c^{\mathrm{F}}_{\mathrm{MTG}\_i}$ is the fuel cost per unit generated energy of MTG; c_{Loss} is the price of loss; $P^{\mathrm{exp}}_{\mathrm{Loss}}$ is the annual power expectation of loss; $T^{\mathrm{use}}_{\mathrm{sys}}$ is the system annual operating hours; $T^{\mathrm{use}}_{\mathrm{sys}} = 8760$ hr.

2) OPERATING RISK OF IMG

The operating risk of an IMG is related to the probability of violating the safe operating limits. It can be formulated as

$$f_2 = \max_{i\in\Omega_{\mathrm{B}}, l\in\Omega_{\mathrm{L}}}(R_{\mathrm{U}i}, R_{\mathrm{S}l}, R_{\mathrm{F}}) \tag{15}$$

where Ω_{B} is the set of bus indices, $\Omega_{\mathrm{L}}$is the set of branch indices, $R_{\mathrm{U}i}$ is the probability of over-limit voltage at bus i, $R_{\mathrm{S}l}$ is the probability of over-limit power transmitted on branch l, R_{F} is the probability of over-limit frequency.

Finally, the multi-objective planning problem of active-reactive power resource is formulated as

$$\min F = \min\{f_1, f_2\} \tag{16}$$

B. CONSTRAINTS

The constraints include active-reactive power resource planning constraints, IMG security operating constraints and operating constraints of equipment, which are explained in detail in the following subsections.

1) POWER FLOW EQUATIONS

Equation (17) represents the power balance in an IMG:

$$\begin{cases} P_{\mathrm{C}i} + P_{\mathrm{D}i} - P_{\mathrm{L}i} - U_j\sum_{j=1}^{n}U_j(G_{ij}\cos\delta_{ij} + B_{ij}\sin\delta_{ij}) = 0 \\ Q_{\mathrm{C}i} + Q_{\mathrm{D}i} - Q_{\mathrm{L}i} - U_j\sum_{j=1}^{n}U_j(G_{ij}\sin\delta_{ij} - B_{ij}\cos\delta_{ij}) = 0 \end{cases} \tag{17}$$

where U_i, U_j are the voltage magnitude of bus i and bus j, respectively; G_{ij}, B_{ij} are the real part and imaginary part of node admittance matrix; δ_{ij} is the voltage phase angle difference of bus i and bus j.

2) RELATIONSHIP BETWEEN ESS MAXIMUM CHARGE/DISCHARGE POWER AND CAPACITY

In practice, the capacity of ESS configuration usually needs to meet the requirement of continuous operating for 3-4 hr under the maximum charge/discharge power. Besides, as a single energy storage unit has certain linear relationship between its capacity and its maximum charge/discharge power, the capacity of the ESS that consists of multiple energy storage units is also assumed to have linear relationship with its maximum output power:

$$E^{\mathrm{r}}_{\mathrm{ESS}\_i} = P^{\mathrm{max}}_{\mathrm{ESS}\_i}T_{\mathrm{con}} \tag{18}$$

where $P^{\mathrm{max}}_{\mathrm{ESS}\_i}$ and T_{con} are the ESS maximum charge/discharge power and continuous operating hours in the maximum charge/discharge power, respectively.

3) INSTALLATION CAPACITY

The installation capacity of DG, ESS, DSTATCOM is limited by (19), and (20) indicates the relationship between the

installation capacity and the installation numbers:

$$\begin{cases} 0 \le P_{\mathrm{MTG}\_i} \le P^{\mathrm{r}}_{\mathrm{MTG}\_i} \\ 0 \le P_{\mathrm{WTG}\_i} \le P^{\mathrm{r}}_{\mathrm{WTG}\_i} \\ 0 \le P_{\mathrm{PVG}\_i} \le P^{\mathrm{r}}_{\mathrm{PVG}\_i} \\ -P^{\max}_{\mathrm{ESS}\_i} \le P_{\mathrm{ESS}\_i} \le P^{\max}_{\mathrm{ESS}\_i} \\ -Q^{\mathrm{r}}_{\mathrm{DS}\_i} \le Q_{\mathrm{DS}\_i} \le Q^{\mathrm{r}}_{\mathrm{DS}\_i} \end{cases} \tag{19}$$

$$\begin{cases} Q_{\mathrm{MTG}\_i} = P_{\mathrm{MTG}\_i} \tan(\varphi_{\mathrm{MTG}}) \\ Q_{\mathrm{WTG}\_i} = P_{\mathrm{WTG}\_i} \tan(\varphi_{\mathrm{WTG}}) \\ Q_{\mathrm{PVG}\_i} = P_{\mathrm{PVG}\_i} \tan(\varphi_{\mathrm{PVG}}) \end{cases} \tag{20}$$

where $P^{\max}_{\mathrm{MTG}\_i}$, $P^{\max}_{\mathrm{WTG}\_i}$, $P^{\max}_{\mathrm{PVG}\_i}$, $E^{\max}_{\mathrm{ESS}\_i}$, $Q^{\max}_{\mathrm{DS}\_i}$ are the maximum allowable installation capacity of MTG, WTG, PVG, ESS, DSTATCOM at bus i, respectively; $P^{\mathrm{r}}_{\mathrm{MTG}\_i0}$, $P^{\mathrm{r}}_{\mathrm{WTG}\_i0}$, $P^{\mathrm{r}}_{\mathrm{PVG}\_i0}$, $E^{\mathrm{r}}_{\mathrm{ESS}\_i0}$, $Q^{\mathrm{r}}_{\mathrm{DS}\_i0}$ respectively represent the rated capacity of single MTG, single WTG, single PVG, single ESS and single DSTATCOM at bus i; a_i, b_i, c_i, d_i, e_i are the installation numbers of MTG, WTG, PV, ESS, DSTATCOM at bus i, respectively.

4) OUTPUT POWER CONSTRAINTS

Equation (21) limits the active power of DG and ESS and the reactive power of DSTATCOM. Equation (22) describes the relationship between active power and reactive power of DG:

$$\begin{cases} 0 \le P_{\mathrm{MTG}\_i} \le P^{\mathrm{r}}_{\mathrm{MTG}\_i} \\ 0 \le P_{\mathrm{WTG}\_i} \le P^{\mathrm{r}}_{\mathrm{WTG}\_i} \\ 0 \le P_{\mathrm{PVG}\_i} \le P^{\mathrm{r}}_{\mathrm{PVG}\_i} \\ -P^{\max}_{\mathrm{ESS}\_i} \le P_{\mathrm{ESS}\_i} \le P^{\max}_{\mathrm{ESS}\_i} \\ -Q^{\mathrm{r}}_{\mathrm{DS}\_i} \le Q_{\mathrm{DS}\_i} \le Q^{\mathrm{r}}_{\mathrm{DS}\_i} \end{cases} \tag{21}$$

$$\begin{cases} Q_{\mathrm{MTG}\_i} = P_{\mathrm{MTG}\_i} \tan(\varphi_{\mathrm{MTG\_i}}) \\ Q_{\mathrm{WTG}\_i} = P_{\mathrm{WTG}\_i} \tan(\varphi_{\mathrm{WTG\_i}}) \\ Q_{\mathrm{PVG}\_i} = P_{\mathrm{PVG}\_i} \tan(\varphi_{\mathrm{PVG\_i}}) \end{cases} \tag{22}$$

where P_{MTG_i}, P_{WTG_i}, P_{PVG_i}, P_{ESS_i}, Q_{DS_i} are the active power of MTG, WTG, PVG, ESS and the reactive power of DSTATCOM at bus i, respectively. Q_{MTG_i}, Q_{WTG_i}, Q_{PVG_i} are the reactive power of MTG, WTG, PVG at bus i, respectively; $\varphi_{\mathrm{MTG\_i}}$, $\varphi_{\mathrm{WTG\_i}}$, $\varphi_{\mathrm{PVG\_i}}$ are the power factor angles of MTG, WTG, PVG at bus$i$, respectively.

5) SECURITY OPERATING CHANCE CONSTRAINTS

Equation (23) indicates that the operation should be kept at a high probability that bus voltage, branch power and system frequency are within the safe operating limits:

$$\begin{cases} \Pr\{U_{i\min} \le U_i \le U_{i\max}\} \ge \gamma_{\mathrm{U}} \\ \Pr\{0 \le S_l \le S_{l\max}\} \ge \gamma_{\mathrm{S}} \\ \Pr\{f_{\min} \le f \le f_{\max}\} \ge \gamma_{\mathrm{F}} \end{cases} \tag{23}$$

where $\Pr\{\cdot\}$ represents the probability of the inequality in$\{\cdot\}$; S_l represents the apparent power of branch$l$; $S^{\max}_l$ represents the maximum allowable apparent power at branch l; γ_U, γ_S, γ_F are the confidence of voltage, branch power and frequency, respectively.

C. METHODOLOGY

The planning model proposed above is a complex integer nonlinear multi-objective optimization model with chance constraints. NSGA-II is widely used to solve multi-objective optimization models because of its superior optimization performance and better compatibility [37]–[39]. In view of the objective function f_2 and security operating chance constraints of the model, the proposed PLFCM for decentralized droop-controlled IMG is embedded in NSGA-II to solve the model. Thus, the Pareto solution set of active-reactive resources considering the correlation among the uncertainty factors are obtained. The flow chart of the algorithm is shown in Fig. 1.

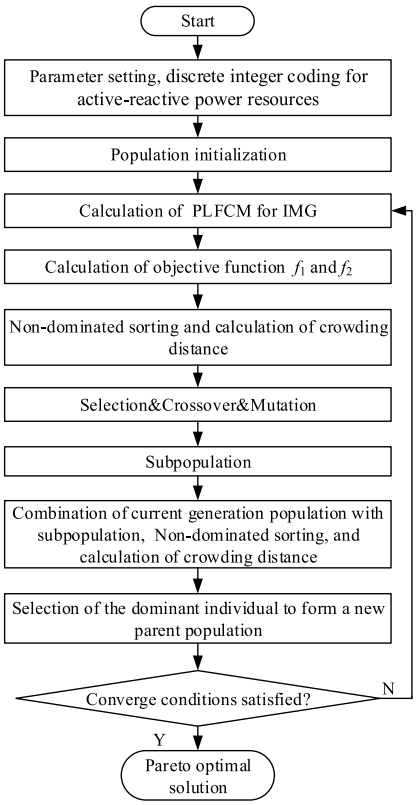

FIGURE 1. Flowchart of the proposed algorithm.

In this paper, the max-min method [39] is used to select the best planning scheme. For each solution X_s in the Pareto solution set, the value of formula (24) can be calculated, which shows the ability of solution X_s in minimising the objective function f_k.

$$\max_{s=1}^{N_{\mathrm{P}}} \left\{ \min_{k=1}^{N_{\mathrm{O}}} \left[\frac{f_k^{\max} - f_k(X_s)}{f_k^{\max} - f_k^{\min}} - \mu_k^{\mathrm{ref}} \right] \right\} \tag{24}$$

where N_{O} is the number of objective functions, N_{P} is the number of the solutions of the Pareto solution set, $f_k^{\max}$ and $f_k^{\min}$ are the maximum and minimum values of the objective function f_k among all the solutions in the Pareto set, μ_k^{ref} is the minimum required satisfaction for the objective function f_k, which is determined by the decision makers

according to their preference. If the decision-makers have no obvious preference for any objective, $\mu_k^{\text{ref}} = 0$.

IV. CASE STUDIES

The proposed PLFCM and the multi-objective planning model of active-reactive power resources for decentralized droop-controlled IMGs are applied to the IEEE 33-bus test system (Fig.2). The technical data of this network can be found in [40]. Bus 1 is disconnected from the main network to form an IMG.

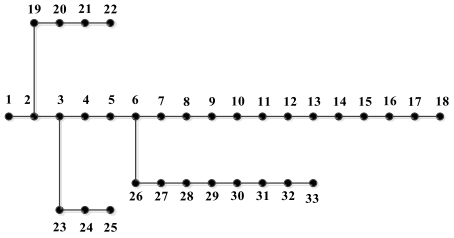

FIGURE 2. IEEE 33-bus test system.

The PDF of load follows the normal distribution, the mean values of the load are based on the data of IEEE-33 bus test system, the standard deviation of load are set to 10% of the mean. The proportions of constant impedance load, constant current load and constant power load are 0.3, 0.3, 0.4, respectively. The frequency sensitivity coefficients for active and reactive power load are $k_{\text{Lp}i} = 2$, $k_{\text{Lq}i} = 2$. The safe operating limits of frequency and voltage for the IMG are set at $f_{\max} = 1.004$ p.u., $f_{\min} = 0.996$ p.u., $U_{\max} = 1.05$ p.u., and $U_{\min} = 0.95$ p.u. The PVG output power follows the Beta distribution and the shape parameters are assumed to be $\alpha = 1.693$ and $\beta = 5.162$. The WTG output power follows the Weibull distribution and the shape parameters are assumed to be $k = 2.94$ and $c = 3.03$. The correlation coefficient among PVG is $\rho_{\text{pp}} = 0.7$, the correlation coefficient among WTG is $\rho_{\text{ww}} = 0.4$, and the correlation coefficients between WTG and PVG are $\rho_{\text{pw}} = \rho_{\text{pw}} = -0.5$.

The algorithms are developed in MATLAB R2013a and implemented in a PC having the following specifications: Intel Core i5-4460 3.2GHz CPU, 4 GB RAM, running under MS Windows 7 Pro version2009.

A. VERIFICATION OF THE CORRECTNESS OF PLFCM FOR IMGs

This case is designed to analyse and verify the validity of the proposed PLFCM for IMGs. MTG, PVG, WTG, ESS and DSTATCOM are integrated to the IEEE 33–bus system, the capacity and location of which are attached in Table 4 in Appendix B.

MCS is commonly used as a benchmark method to verify the accuracy of other PLF methods [13]–[17]. MCS with 10000 samples is utilized to evaluate the accuracy of the proposed PLFCM. Figs. 3 and 4 show the PDFs and CDFs of frequency and voltage magnitude at bus 4, respectively. Table 1 lists the mean value and the standard deviation

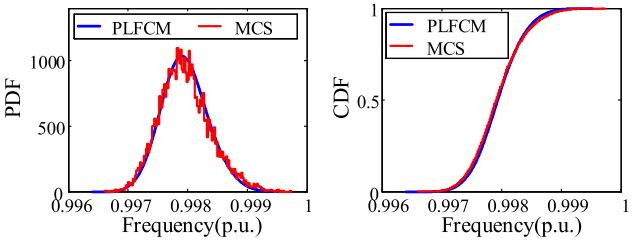

FIGURE 3. PDF and CDF of frequency.

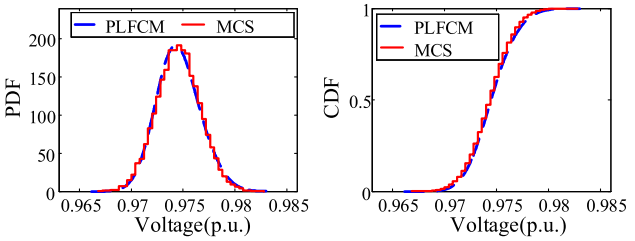

FIGURE 4. PDF and CDF of voltage magnitude at bus 4.

obtained by the proposed method in comparison with MCS. Besides, the computational time of PLFCM is 0.06 s whereas MCS is 163.27 s.

As it can be seen from the results, the PLFCM can provide accurate approximation to the PDF and CDF, whereas the computational time is much less than MCS. According to Table 1, the errors of PLFCM are acceptable, and the accuracy could meet the engineering application requirements. Therefore, the proposed PLFCM for IMG has a significant advantage in computational time under the premise of allowable error, and it is feasible to on-line computation.

TABLE 1. Comparison of the results for voltage magnitude and frequency.

variable		mean		standard deviation	
Voltage magnitude (p.u.)	bus	MCS	PLFCM	MCS	PLFCM
	1	0.98204	0.98207	0.00237	0.00249
	4	0.97454	0.97458	0.00209	0.00211
	18	0.96073	0.96079	0.00466	0.00554
	29	0.99330	0.99332	0.00201	0.00233
	33	1.00560	1.00561	0.00299	0.00351
Frequency(p.u.)		0.99795	0.99795	0.00043	0.00040

B. SIMULATION OF MULTI-OBJECTIVE PLANNING MODEL OF ACTIVE-REACTIVE POWER RESOURCES FOR DECENTRALIZED DROOP-CONTROLLED IMGs

The proposed multi-objective planning model of active-reactive power resources for decentralized droop-controlled IMGs is validated in this case study. The parameters of this case are attached in Table 5 in Appendix B.

1) ANALYSIS ON THE COMPLEMENTARY CORRELATION BETWEEN WIND POWER AND PHOTOVOLTAIC POWER

According to the proposed optimal planning model of active-reactive power resources for decentralized droop-controlled IMGs in Section III, PLFCM for decentralized droop-controlled IMGs is embedded in NSGA-II, which is used to

obtain the Pareto optimal solution. Considering that normally there is some complementary correlation between the solar radiation and the wind speed [35], the impact of the complementary correlation on optimal planning is also investigated in this case, where the Pareto fronts are obtained with and without considering correlation between wind power and photovoltaic power, and are compared as depicted in Fig. 5.

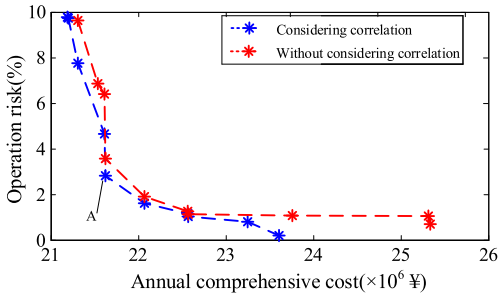

FIGURE 5. Pareto fronts with and without considering correlation.

According to Fig. 5, the Pareto front considering correlation is lower than without considering correlation, which means that the planning result is better if the complementary correlation between wind power and photovoltaic power is considered. The planning result also confirms the positive role of complementary correlation between wind power and photovoltaic power in the planning and operation of IMG. Hence, in multi-objective planning, it is necessary to consider the complementary correlation between wind power and photovoltaic power, which can make the planning results more reasonable.

2) ANALYSIS OF PLANNING SCHEME

The Pareto front plotted in blue in Fig. 5 is obtained when the correlation between wind power and photovoltaic power is considered. Assuming that decision-makers have no obvious preference for any target, we have $\mu_1^{\text{ref}} = \mu_2^{\text{ref}} = 0$. The best solution is found using (24), which is the solution at point A. The planning scheme for this solution is labelled as scheme 3 and the results are shown in Table 2. Correspondingly, the case of minimum annual comprehensive cost is labelled as scheme 1 and the case of minimum operating risk is labelled scheme 2. Thus, three typical planning schemes are formed. The annual comprehensive cost and the operating risk of the three planning schemes are shown in Table 3.

TABLE 2. Planning results of scheme 3.

Bus	MTG (kW)	WTG (kW)	PVG (kW)	ESS (kWh)	DSTACOM (kvar)
1	800	0	800	700	700
7	800	0	600	300	600
12	0	0	800	300	600
18	200	800	0	200	0
22	0	300	0	0	0
29	0	800	0	0	0
33	800	700	0	0	0

TABLE 3. Annual comprehensive cost and operating risk of the three planning schemes.

Scheme	Annual comprehensive cost ($\times 10^6$ ¥)	Operating risk (%)
1	21.187	9.7719
2	23.605	0.1879
3	21.621	2.8219

The three planning schemes are compared as follows. Scheme 1 concentrates on controlling the annual comprehensive cost. As a result, the capacity of MTG, ESS and DSTATCOM is less than that in other schemes, but the operating risk reaches 9.7719%. Scheme 2 has a strong active-reactive regulating ability, for the reason that the capacity of active and reactive power regulating equipment is sufficient. It leads to a result that the operating risk can be reduced to a minimum of 0.1879%, but the comprehensive cost increases to 23.605×10^6 ¥. For scheme 3, its annual comprehensive cost is merely 0.434×10^6 ¥higher than that of scheme 1, but the operating risk can be reduced to 2.8219%, which has the best coordinating result.

Fig. 6 represents the PDF of frequency and Fig. 7 reflects the system voltage level. As shown in Fig. 6, the frequency variation in scheme 2 is less than that in other schemes, which is basically within the safe operating limit. The PDF of frequency of scheme 1 is more disperse and has a certain probability of over-limit. Compared with scheme 1, the probability of over-limit frequency in scheme 3 is lower. In Fig. 7, the solid lines represent the means of the bus voltages, and the dashed lines represent the 90% confidence intervals frontiers. According to this figure, the least voltage fluctuation is found in scheme 2, whose voltage level is higher than other schemes

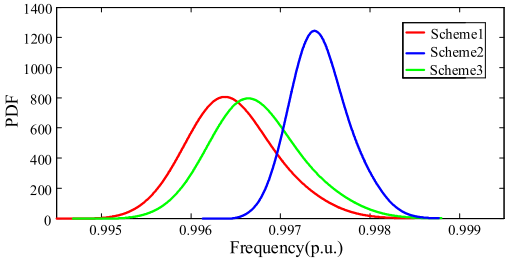

FIGURE 6. The PDFs of the frequency in the three planning schemes.

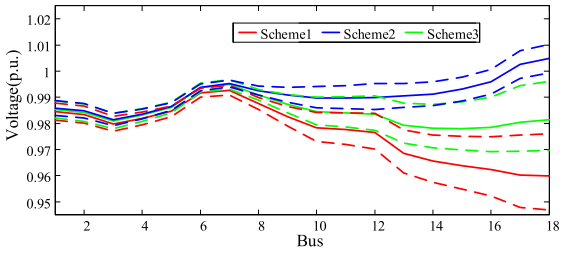

FIGURE 7. The means and 90% confidence intervals of the voltages at bus 1-18 in the three planning schemes.

as well. For scheme 3, the voltage level and the fluctuation is within the safe operating interval, which means that the voltage quality of scheme 3 is acceptable. The range of voltage fluctuation in scheme 1 is the largest, meanwhile, some bus voltages have the risk of over-limit. Overall, scheme 2 shows the best ability of frequency and voltage control, closely followed by scheme 3, and its operating risk is acceptable.

3) COMPARISON AND ANALYSIS WITH ROBUST OPTIMIZATION

The proposed planning method of active-reactive power resources is compared with robust optimization in this subsection. Robust optimization is one of the common methods to deal with uncertainty problems in power systems. It finds the optimal planning solution in the worst case as uncertain parameters vary within their associated uncertainty intervals [26]. The robust optimization targeting at the minimum annual comprehensive cost, is solved by the genetic algorithm whose parameters are the same as listed in Subsection B of Section IV. Hence the optimal planning scheme under the worst case can be obtained, which is attached in Table 6 in Appendix B.

The annual comprehensive cost of the robust optimization solution is increased by 25.6% from scheme 3 to 27.153×10^6 ¥. This increase represents the cost of robustness being paid to strengthen the IMG against the uncertain variations of load and DG of the worst case. Further analysis from the deployment of active-reactive resources, the planning scheme of the robust optimization is more inclined to reduce the configuration capacity of PVG and WTG, and meanwhile to increase the configuration capacity of MTG and ESS to ensure that the safe operating limits are met under the worst case. The above analysis shows that: 1) As robust optimization is concerned with the feasibility of the solution under the worst case, its planning scheme is highly conservative; 2) The proposed planning method based on PLF use the objective function and the chance constraints to control the operating risk. The method not only concerns the feasibility of the solution under an uncertainty environment, but also pays attention to the economy of the planning scheme. Furthermore, the operating risk of the corresponding planning scheme can be quantified directly as well.

4) ANALYSIS OF THE UNITS QUITTING OPERATION

Scheme 3 mentioned in Subsection (b) is selected as the basic case in this subsection. 5 scenarios are designed for the analysis of the units quitting operation.

Scenario 1: MTG at bus 18 quit operation;
Scenario 2: PVG at bus 12 quit operation;
Scenario 3: WTG at bus 33 quit operation;
Scenario 4: ESS at bus 7 quit operation;
Scenario 5: DSTATCOM at bus 7 quit operation.

In scenarios 1-4, the units quitting operation mainly influences the active power of the IMG. Considering that the frequency is related to the active power, the PDFs of the frequency are compared and depicted in Fig. 8. On the other hand, the units quitting operation in scenario 5 mainly impacts reactive power and bus voltage. The comparison of mean and 90% confidence intervals in scenario 5 is shown in Fig. 9. The analysis of the units quitting operation is given as follows.

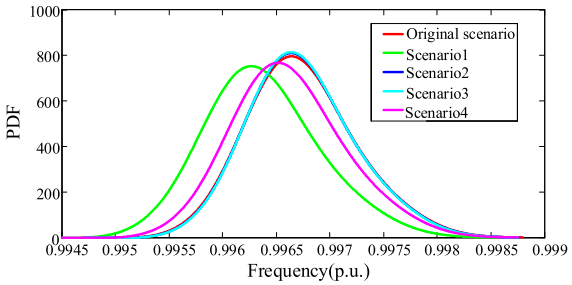

FIGURE 8. Comparison of PDFs of frequency in scenario1-4.

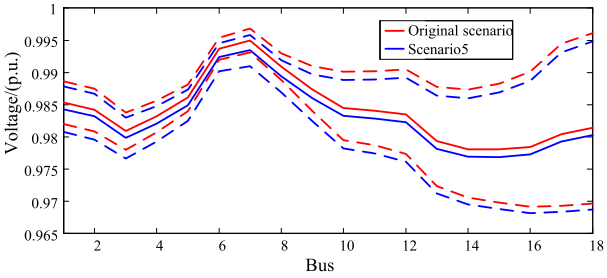

FIGURE 9. Comparison of means and 90% confidence intervals in scenario 5.

(1) When PVG or WTG units quit operation due to failure or some other reasons, the mean of frequency will decline, whereas the fluctuation of frequency will also decrease slightly, however, the impact on the PDF of frequency is not particularly obvious. The reason for the inconspicuous impact on PDF is that the output power of PVG follows Beta distribution and WTG follows Weibull distribution, it is always difficult for PVG and WTG to achieve the rated power output, even commonly operate at a lower power. Hence sufficient capacity of MTG or ESS are configured in the planning scheme to support the load and reduce the operating risk. In conclusion, PVG or WTG quitting operation will lead to frequency decline, if the frequency is within the safe operating limit, the IMG can continue to operate, otherwise load-shedding should be considered to ensure the frequency is within the safe operating interval.

(2) The PDF of frequency in scenario 1 and scenario 4 shows that the probability of over lower limit frequency is increased due to insufficient active power resources, and the range of fluctuation frequency is increased as well. The simulation results fully reflect that MTG and ESS play crucial roles in solving the problem of fluctuation and over-limit frequency caused by the uncertainties of PVG and WTG. Thus, redundant configuration can be considered in the MTG and ESS planning scheme if the economic conditions can

be satisfied. In addition, in cases where MTG or ESS quit operation and the IMG has no other spare capacity, load-shedding should be taken to adjust frequency within the safe operating limit.

(3) For scenario 5, the whole voltage level is decreased and the range of fluctuation voltage are increased after DSTATCOM at bus 7 quits operation, but the fluctuation is within the safe operating limit. In cases where DSTATCOM quitting operation will result in voltage decline, if the voltage is over-limit and MTG has sufficient capacity, the power factor of MTG can be reduced to improve its reactive power output, otherwise load-shedding should be considered to maintain the voltage within the safe operating limit.

According to the case studies presented above, the proposed multi-objective coordinated planning model of active-reactive power resources for decentralized droop-controlled IMG can reflect the complementarity of wind power and photovoltaic power, and the planning schemes obtained can coordinate the security and economy of IMG operation.

C. DISCUSSION ON THE ASSUMPTIONS

The assumptions of this paper mainly include:

Assumption A: The output impedance of the active-reactive power resources is assumed to be inductive [10], [30].

Assumption B: The power output of WTG and PVG is assumed that wind speed follows the Weibull distribution, and solar radiation follows the Beta distribution [11]–[14].

Assumption C: The capacity of the ESS is assumed to have linear relationship with its maximum output power.

Two major contributions are emphasized in this paper: 1) PLFCM for decentralized droop-controlled IMGs is proposed; 2) a multi-objective model is proposed for the planning of active-reactive power resources in a decentralized droop-controlled IMG, based on probabilistic load flow. Although the research in this paper is based on the above assumptions, the contributions have the theoretical significance and the value for the engineering application as well. The reasons are as follows.

(1) With respect to the source of the assumptions, they are either based on references (such as assumptions A and B) or engineering practice (such as assumptions A and C). Hence, it can reflect the engineering reality and has the potential of real-world application.

(2) The contributions are not restricted by the assumptions. Such as assumption A, as analysis in the last paragraph of Section II.B, the proposed PLFCM is also appropriate for resistive grids. As for assumption B, the proposed PLFCM is appropriate for other probability distributions that the WTG and PVG follow as well [15], [41]. With regard to assumption C, if the capacity of the ESS does not have linear relationship with its maximum output power, we can add the variables of the maximum output power of ESS to the planning model, so that it is also appropriate to apply the proposed multi-objective coordinated planning model.

Therefore, based on the reasons mentioned above, it is justified to consider that the proposed PLFCM and planning model for decentralized droop-controlled IMGs, have the theoretical significance and the value for the engineering application as well.

V. CONCLUSIONS

Currently, PLF of decentralized droop-controlled IMGs is mainly solved by MCS, which brings huge computational burden. To overcome this, PLFCM considering the correlation of input random variables is proposed. On this basis, a multi-objective coordinated planning model of active-reactive power resources is constructed to control the annual comprehensive cost and handle the operating risk. The conclusions are as follows.

(1) The calculation result of PLFCM is very close to MCS. Unlike MCS, the proposed PLFCM avoids the sampling procedure and repeated simulation, thus shortens the computational time and improves the computational efficiency. Hence it is feasible to be applied in on-line computation and embedded in intelligent optimization algorithms.

(2) The results of numerical case studies show that the proposed optimal planning model of active-reactive power resources can reflect the complementarity of wind power and photovoltaic power, and the obtained planning schemes can coordinate the annual comprehensive cost and the operating risk of an IMG.

(3) Analysis of unit quitting operation shows that MTG and ESS play an important role in frequency controlling of an IMG, thus redundant configuration of MTG and ESS can be taken into account in the planning scheme.

APPENDIX

A. APPENDIX A

The dimensions and expressions of each block matrix of the Jacobian matrix are as follows:

$$\boldsymbol{E}_{(n_{\mathrm{pQ}}+n_{\mathrm{pv}})\times 1} = \frac{\partial \Delta P_i}{\partial f} = -\frac{1}{K_{\mathrm{D}fi}} - P_{\mathrm{LN}i}[A_{\mathrm{p}i}(U_i)^2 + B_{\mathrm{p}i}U_i + C_{\mathrm{p}i}] \bullet k_{\mathrm{Lp}i}$$

$$\boldsymbol{F}_{n_{\mathrm{pQ}}\times 1} = \frac{\partial \Delta Q_i}{\partial f} = -Q_{\mathrm{LN}i}[A_{\mathrm{q}i}(U_i)^2 + B_{\mathrm{q}i}U_i + C_{\mathrm{q}i}] \bullet k_{\mathrm{Lq}i}$$

$$\boldsymbol{H}_{(n_{\mathrm{pQ}}+n_{\mathrm{pv}})\times(n_{\mathrm{pQ}}+n_{\mathrm{pv}})-1} = \frac{\partial \Delta P_i}{\partial \delta_j} = \begin{cases} -U_iU_j(G_{ij}\sin\delta_{ij} - B_{ij}\cos\delta_{ij}) & i \neq j \\ U_i^2B_{ii} + Q_i & i = j \end{cases}$$

$$\boldsymbol{M}_{n_{\mathrm{pQ}}\times(n_{\mathrm{pQ}}+n_{\mathrm{pv}}-1)} = \frac{\partial \Delta Q_i}{\partial \delta_j} = \begin{cases} U_iU_j(G_{ij}\cos\delta_{ij} + B_{ij}\sin\delta_{ij}) & i \neq j \\ U_i^2G_{ii} - P_i & i = j \end{cases}$$

$$\boldsymbol{N}_{(n_{\mathrm{pQ}}+n_{\mathrm{pv}})\times n_{\mathrm{pQ}}} = \frac{\partial \Delta P_i}{U\delta_j} = \begin{cases} -U_i(G_{ij}\cos\delta_{ij} + B_{ij}\sin\delta_{ij}) & i \neq j \\ -P_{\mathrm{LN}i}(2A_{\mathrm{p}i}U_i + B_{\mathrm{p}i}) \\ \quad \times[1 + k_{\mathrm{Lp}i}(f - f_N)] - U_iG_{ii} - \frac{P_i}{U_i} & i = j \end{cases}$$

TABLE 4. Capacity and location of the case in subsection A of section IV.

Location	MTG (kW)	WTG (kW)	PVG (kW)	ESS (kWh)	DSTATCOM (kvar)
1	800	-	800	-	-
7	-	-	600	-	800
12	-	-	600	-	-
18	-	500	-	2000	-
22	800	500	-	-	-
29	800	500	-	-	-
33	800	500	-	-	-

TABLE 5. Parameters of the case in subsection B of section IV.

Parameters	Value	Parameters	Value
Candidate buses for MTG	bus 1, 7, 18, 29, 33	Candidate buses for PVG	bus 1, 7, 12
Candidate buses for WTG	bus 18, 22, 29, 33	Candidate buses for ESS	Bus 1, 7, 12, 18, 22, 29, 33
Candidate buses for DSTATCOM	bus 1, 7, 12	$\cos\varphi_{WTG}$, $\cos\varphi_{PVG}$, $\cos\varphi_{MTG}$	1 1 0.8
$P^{r}_{WTG\_i0}$, $P^{r}_{PVG\_i0}$, $P^{r}_{MTG\_i0}$	100kW 100kW 100kW	y_{MTG}, y_{WTG}, y_{PVG}, y_{ESS}, y_{DS}	20
$E^{r}_{ESS\_i0}$	100kWh	$Q^{r}_{DS\_i0}$	100kvar
$P^{max}_{MTG\_i}$, $P^{max}_{xWTG\_i}$, $P^{max}_{PVG\_i}$	800kW 800kW 800kW	$E^{max}_{ESS\_i}$	800kWh
$Q^{max}_{DS\_i}$	800kvar	$c^{F}_{MTG\_i}$	0.6¥/kWh
c_{Loss}	0.5¥/kWh	d	0.06
S^{max}_{i}	7MVA	γ_U,γ_S,γ_F	0.9
$c^{I}_{MTG\_i}$, $c^{I}_{WTG\_i}$, $c^{I}_{PVG\_i}$, $c^{I}_{ESS\_i}$, $c^{I}_{DS\_i}$	6500¥/kW, 7800¥/kW, 8200¥/kW, 6000¥/kWh, 1000¥/kW	$c^{OM}_{MTG\_i}$, $c^{OM}_{WTG\_i}$, $c^{OM}_{PVG\_i}$, $c^{OM}_{ESS\_i}$, $c^{OM}_{DS\_i}$	0.08¥/kWh, 0.3¥/kWh, 0.3¥/kWh, 1000¥/kWh*yr, 100¥/kvar*yr
T_{con}	4h		

TABLE 6. Planning results of robust optimization.

Bus	MTG (kW)	WTG (kW)	PVG (kW)	ESS (kWh)	DSTACOM (kvar)
1	800	0	500	800	800
7	800	0	400	800	800
12	0	0	500	0	400
18	800	0	0	600	0
22	0	800	0	800	0
29	800	0	0	800	0
33	800	500	0	0	0

$$\boldsymbol{L}_{(n_{pQ}+n_{pQ})} = \frac{\partial \Delta Q_i}{\partial U_j} = \begin{cases} -U_i(G_{ij}\sin\delta_{ij} - B_{ij}\cos\delta_{ij}) & i \neq j \\ -\dfrac{1}{K_D Ui} - Q_{LNi}(2A_{qi}U_i + B_{qi}) \\ \quad \times[1 + k_{Lqi}(f - f_N)] - U_i B_{ii} - \dfrac{Q_i}{U_i} & i = j \end{cases}$$

where n_{PQ} and n_{PV} are the number of PQ bus-type and PV bus-type respectively; K_{Dfi}, K_{Dui} respectively represent droop coefficient of P-f, Q-U of droop bus-type; A_{pi}, B_{pi}, C_{pi}, A_{qi}, B_{qi}, C_{qi} are the percentage of constant impedance modeling, constant current modeling and constant power modelling for active-reactive load respectively;P_{LNi}, Q_{LN} respectively represent the active and reactive load under rated conditions.

B. APPENDIX B

The capacity and location of DG, ESS and DSTATCOM of the case in Subsection A of Section IV is shown in Table 4. Parameters of the case in Subsection B of Section IV are given in Table 5. The planning scheme based on robust optimization is shown in Table 6.

REFERENCES

[1] M. Sedghi, A. Ahmadian, and M. Aliakbar-Golkar, "Optimal storage planning in active distribution network considering uncertainty of wind power distributed generation," *IEEE Trans. Power Syst.*, vol. 31, no. 1, pp. 304–316, Jan. 2016.
[2] L. Guo *et al.*, "Energy management system for stand-alone wind-powered-desalination microgrid," *IEEE Trans. Smart Grid*, vol. 7, no. 2, pp. 1079–1087, Mar. 2016.
[3] Y. Xiang, J. Liu, and Y. Liu, "Robust energy management of microgrid with uncertain renewable generation and load," *IEEE Trans. Smart Grid*, vol. 7, no. 2, pp. 1034–1043, Mar. 2016.
[4] Y. Kuang *et al.*, "A review of renewable energy utilization in islands," *Renew. Sustain. Energy Rev.*, vol. 59, pp. 504–513, Jun. 2016.
[5] M. M. A. Abdelaziz, H. E. Farag, E. F. El-Saadany, and Y. A.-R. I. Mohamed, "A novel and generalized three-phase power flow algorithm for islanded microgrids using a Newton trust region method," *IEEE Trans. Power Syst.*, vol. 28, no. 1, pp. 190–201, Feb. 2013.
[6] A. A. Eajal, M. A. Abdelwahed, E. F. El-Saadany, and K. Ponnambalam, "A unified approach to the power flow analysis of AC/DC hybrid microgrids," *IEEE Trans. Sustain. Energy*, vol. 7, no. 3, pp. 1145–1158, Jul. 2016.
[7] A. G. Tsikalakis and N. D. Hatziargyriou, "Centralized control for optimizing microgrids operation," *IEEE Trans. Energy Convers.*, vol. 23, no. 1, pp. 241–248, Mar. 2008.
[8] A. Elrayyah, Y. Sozer, and M. E. Elbuluk, "A novel load-flow analysis for stable and optimized microgrid operation," *IEEE Trans. Power Del.*, vol. 29, no. 4, pp. 1709–1717, Aug. 2014.
[9] X. Wu, C. Shen, and R. Iravani, "Feasible range and optimal value of the virtual impedance for droop-based control of microgrids," *IEEE Trans. Smart Grid*, vol. 8, no. 3, pp. 1242–1251, May 2017.
[10] F. Mumtaz, M. H. Syed, M. Al Hosani, and H. H. Zeineldin, "A novel approach to solve power flow for islanded microgrids using modified Newton Raphson with droop control of DG," *IEEE Trans. Sustain. Energy*, vol. 7, no. 2, pp. 493–503, Apr. 2016.
[11] S. Zhang, H. Cheng, L. Zhang, M. Bazargan, and L. Yao, "Probabilistic evaluation of available load supply capability for distribution system," *IEEE Trans. Power Syst.*, vol. 28, no. 3, pp. 3215–3225, Aug. 2013.
[12] Z. Pan, M. Shi, Y. Wu, J. Liu, and X. Tong, "Probabilistic load flow of islanded microgrid with droop-controlled distributed generations," in *Proc. IEEE PES Asia–Pacific Power Energy Conf.*, Xi'an, China, Oct. 2016, pp. 536–540.
[13] V. A. Evangelopoulos and P. S. Georgilakis, "Optimal distributed generation placement under uncertainties based on point estimate method embedded genetic algorithm," *IET Gener., Transmiss. Distrib.*, vol. 8, no. 3, pp. 389–400, Mar. 2014.
[14] X. Wang, Y. Gong, and C. Jiang, "Regional carbon emission management based on probabilistic power flow with correlated stochastic variables," *IEEE Trans. Power Syst.*, vol. 30, no. 2, pp. 1094–1103, Mar. 2015.
[15] A. Tamtum, A. Schellenberg, and D. W. Rosehart, "Enhancements to the cumulant method for probabilistic optimal power flow studies," *IEEE Trans. Power Syst.*, vol. 24, no. 4, pp. 1739–1746, Nov. 2009.
[16] M. Fan, V. Vittal, G. T. Heydt, and R. Ayyanar, "Probabilistic power flow studies for transmission systems with photovoltaic generation using cumulants," *IEEE Trans. Power Syst.*, vol. 27, no. 4, pp. 2251–2261, Nov. 2012.
[17] J. Usaola, "Probabilistic load flow with wind production uncertainty using cumulants and Cornish–Fisher expansion," *Int. J. Elect. Power Energy Syst.*, vol. 31, no. 9, pp. 474–481, 2009.
[18] N. Soleimanpour and M. Mohammadi, "Probabilistic load flow by using nonparametric density estimators," *IEEE Trans. Power Syst.*, vol. 28, no. 4, pp. 3747–3755, Nov. 2013.
[19] D. Villanueva, A. E. Feijóo, and J. L. Pazos, "An analytical method to solve the probabilistic load flow considering load demand correlation using the DC load flow," *Electr. Power Syst. Res.*, vol. 110, pp. 1–8, May 2014.

[20] S. Liu, P. X. Liu, X. Wang, Z. Wang, and W. Meng, "Effects of correlated photovoltaic power and load uncertainties on grid-connected microgrid day-ahead scheduling," *IET Gener., Transmiss. Distrib.*, vol. 11, no. 14, pp. 3620–3627, Oct. 2017.

[21] G. Xue, Y. Zhang, and Y. Liu, "Multi-objective optimization of a microgrid considering load and wind generation uncertainties," *Int. Rev. Elect. Eng.*, vol. 7, no. 6, pp. 6225–6234, 2012.

[22] J. Liu, X. Hao, P. Cheng, W. Fang, and S. Niu, "A parallel probabilistic load flow method considering nodal correlations," *Energies*, vol. 9, no. 12, pp. 1041–1056, 2016.

[23] R. Majumder, "Reactive power compensation in single-phase operation of microgrid," *IEEE Trans. Ind. Electron.*, vol. 60, no. 4, pp. 1403–1416, Apr. 2013.

[24] S. Mashayekh and K. L. Butler-Purry, "An integrated security-constrained model-based dynamic power management approach for isolated microgrids in all-electric ships," *IEEE Trans. Power Syst.*, vol. 30, no. 6, pp. 2934–2945, Nov. 2015.

[25] Z. Wang, Y. Chen, S. Mei, S. Huang, and Y. Xu, "Optimal expansion planning of isolated microgrid with renewable energy resources and controllable loads," *IET Renew. Power Gener.*, vol. 11, no. 7, pp. 931–940, Jun. 2017.

[26] A. Khodaei, S. Bahramirad, and M. Shahidehpour, "Microgrid planning under uncertainty," *IEEE Trans. Power Syst.*, vol. 30, no. 5, pp. 2417–2425, Sep. 2015.

[27] J. Mitra, M. R. Vallem, and C. Singh, "Optimal deployment of distributed generation using a reliability criterion," *IEEE Trans. Ind. Appl.*, vol. 52, no. 3, pp. 1989–1997, May/Jun. 2016.

[28] C. Wang, B. Jiao, L. Guo, K. Yuan, and B. Sun, "Optimal planning of stand-alone microgrids incorporating reliability," *J. Mod. Power Syst. Clean Energy*, vol. 2, no. 3, pp. 195–205, 2014.

[29] C. Chen, S. Duan, T. Cai, B. Liu, and G. Hu, "Optimal allocation and economic analysis of energy storage system in microgrids," *IEEE Trans. Power Electron.*, vol. 26, no. 10, pp. 2762–2773, Oct. 2011.

[30] E. Rokrok and M. E. H. Golshan, "Adaptive voltage droop scheme for voltage source converters in an islanded multibus microgrid," *IET Gener., Transmiss. Distrib.*, vol. 4, no. 5, pp. 562–578, May 2010.

[31] J. Zhao, X. Lyu, Y. Fu, X. Hu, and F. Li, "Coordinated microgrid frequency regulation based on DFIG variable coefficient using virtual inertia and primary frequency control," *IEEE Trans. Energy Convers.*, vol. 31, no. 3, pp. 833–845, Sep. 2016.

[32] J. A. Suul, S. D'Arco, and G. Guidi, "Virtual synchronous machine-based control of a single-phase bi-directional battery charger for providing vehicle-to-grid services," *IEEE Trans. Ind. Appl.*, vol. 52, no. 4, pp. 3234–3244, Jul./Aug. 2016.

[33] C. Li, S. K. Chaudhary, M. Savaghebi, J. C. Vasquez, and J. M. Guerrero, "Power flow analysis for low-voltage AC and DC microgrids considering droop control and virtual impedance," *IEEE Trans. Smart Grid*, vol. 8, no. 6, pp. 2754–2764, Nov. 2017.

[34] C. Zhang, Y. Ding, C. Zhang, Y. Xue, and J. Østergaard, "Uncertainty-averse TRANSCO planning for accommodating renewable energy in CO_2 reduction environment," *J. Mod. Power Syst. Clean Energy*, vol. 3, no. 1, pp. 24–32, 2015.

[35] H. Wu, J. Xu, Y. Ji, and M. Wu, "Uncertain flow calculations of a distribution network containing DG based on blind number theory," *IET Gener., Transmiss. Distrib.*, vol. 11, no. 6, pp. 1591–1597, Apr. 2017.

[36] Y. Chen, J. Wen, and S. Cheng, "Probabilistic load flow method based on Nataf transformation and latin hypercube sampling," *IEEE Trans. Sustain. Energy*, vol. 4, no. 2, pp. 294–301, Apr. 2013.

[37] F. Abbasi and S. M. Hosseini, "Optimal DG allocation and sizing in presence of storage systems considering network configuration effects in distribution systems," *IET Gener., Transmiss. Distrib.*, vol. 10, no. 3, pp. 617–624, Feb. 2016.

[38] H. A. Mostafa, R. El-Shatshat, and M. M. A. Salama, "Multi-objective optimization for the operation of an electric distribution system with a large number of single phase solar generators," *IEEE Trans. Smart Grid*, vol. 4, no. 2, pp. 1038–1047, Jun. 2013.

[39] A. Soroudi, R. Caire, N. Hadjsaid, and M. Ehsan, "Probabilistic dynamic multi-objective model for renewable and non-renewable distributed generation planning," *IET Gener., Transmiss. Distrib.*, vol. 5, no. 11, pp. 1173–1182, Nov. 2011.

[40] M. E. Baran and F. F. Wu, "Network reconfiguration in distribution systems for loss reduction and load balancing," *IEEE Trans. Power Del.*, vol. 4, no. 2, pp. 1401–1407, Apr. 1989.

[41] M. Fan, V. Vittal, G. T. Heydt, and R. Ayyanar, "Probabilistic power flow analysis with generation dispatch including photovoltaic resources," *IEEE Trans. Power Syst.*, vol. 28, no. 2, pp. 1797–1805, May 2013.

ZEHUAI LIU received the B.E. degree in electrical engineering from the Guangdong University of Technology, Guangzhou, China, in 2011, and the M.S. degree in electrical engineering from the South China University of Technology, Guangzhou, China, in 2016, where he is currently pursuing the Ph.D. degree in electrical engineering with the School of Electric Power.

His research interests include power system control and optimization, and microgrid operation and planning.

JIAHAO YANG received the B.E. and M.S. degrees in electrical engineering from the South China University of Technology, Guangzhou, China, in 2013 and 2016, respectively.

He is currently a Research Assistant with the School of Electrical Engineering, Xiamen University Tan Kah Kee College, Zhangzhou, China. His research interests include power system planning and operation.

YONGJUN ZHANG received the B.E. and Ph.D. degrees in electrical engineering from the South China University of Technology, Guangzhou, China, in 1995 and 2004, respectively.

From 1995 to 2005, he was a Research Assistant, and also an Assistant Professor from 2006 to 2013 with the School of Electric Power, South China University of Technology, where he is currently a Professor. He has authored three books and over 100 articles. His research interests include power system reactive power optimization, distributed generation control and optimization, voltage control, energy saving, and high-voltage direct current transmission.

TIANYAO JI received the B.E. degree in information engineering, the B.A. degree in english, and the M.S. degree in signal and information processing from Xi'an Jiaotong University, Xi'an, China, in 2003, 2003, and 2006, respectively, and the Ph.D. degree in electrical engineering and electronics from the University of Liverpool, Liverpool, U.K., in 2009.

From 2010 to 2011, she was a Research Associate with the University of Liverpool. She is currently an Associate Professor with the School of Electric Power, South China University of Technology, Guangzhou, China. Her research interests include mathematical morphology, signal and information processing, power system protection, and evolutionary computation.

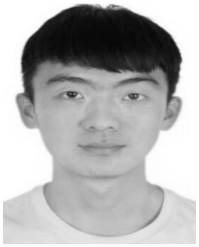

JUNHUANG ZHOU received the B.E. degree in electrical engineering from the South China University of Technology, Guangzhou, China, in 2016, where he is currently pursuing the M.S. degree in electrical engineering with the School of Electric Power. His research interests are power system control and optimization.

ZEXIANG CAI received the B.E. degree in electrical engineering from the Huainan Mineral Institute, Hefei, China, in 1982, the M.S. degree in electrical engineering from the Northeast China Institute of Electrical Power Engineering in 1985, and the Ph.D. degree in electrical engineering from Tsinghua University, Beijing, China, in 1991.

He is currently a Professor with the School of Electric Power Engineering, South China University of Technology, Guangzhou, China. His current research interests include power system stability and control, and power system protective relaying.